Comparative membrane interaction study of viscotoxins A3, A2 and B from mistletoe (*Viscum album*) and connections with their structures

Alexandre COULON*[1], Amor MOSBAH†[1], André LOPEZ*[2], Anne-Marie SAUTEREAU*, Gerhard SCHALLER‡, Konrad URECH‡, Pierre ROUGÉ* and Hervé DARBON†

*Institut de Pharmacologie et de Biologie Structurale, Centre National de la Recherche Scientifique (CNRS) UMR 5089, 205 route de Narbonne, 31077 Toulouse Cedex 4, France, †Architecture et Fonctions des Macromolécules Biologiques, Centre National de la Recherche Scientifique (CNRS) UPR 9039, 31 Chemin Joseph Aiguier, 13402 Marseille, France, and ‡Verein für Krebsforschung, Institut Hiscia, CH-4144 Arlesheim, Switzerland

Viscotoxins A2 (VA2) and B (VB) are, together with viscotoxin A3 (VA3), among the most abundant viscotoxin isoforms that occur in mistletoe-derived medicines used in anti-cancer therapy. Although these isoforms have a high degree of amino-acid-sequence similarity, they are strikingly different from each other in their *in vitro* cytotoxic potency towards tumour cells. First, as VA3 is the only viscotoxin whose three-dimensional (3D) structure has been solved to date, we report the NMR determination of the 3D structures of VA2 and VB. Secondly, to account for the *in vitro* cytotoxicity discrepancy, we carried out a comparative study of the interaction of the three viscotoxins with model membranes. Although the overall 3D structure is highly conserved among the three isoforms, some discrete structural features and associated surface properties readily account for the different affinity and perturbation of model membranes. VA3 and VA2 interact in a similar way, but the weaker hydrophobic character of VA2 is thought to be mainly responsible for the apparent different affinity towards membranes. VB is much less active than the other two viscotoxins and does not insert into model membranes. This could be related to the occurrence of a single residue (Arg^{25}) protruding outside the hydrophobic plane formed by the two amphipathic α-helices, through which viscotoxins are supposed to interact with plasma membranes.

Key words: fluorescence polarization, isochoric measurements, mistletoe, NMR three-dimensional structures, peptide–membrane interaction, viscotoxin.

INTRODUCTION

Thionins constitute a homogeneous group of structurally related plant proteins of low molecular mass which have been widely investigated owing to their antimicrobial properties and toxic effects on mammalian cell lines [1–3]. Thionins isolated from mistletoe (*Viscum album*), also referred to as viscotoxins, consist of polypeptides of 46 amino acid residues (Figure 1). These basic proteins exhibit a net positive charge (+5 or +6) and contain three strictly conserved disulphide bridges that stabilize their three-dimensional (3D) structures [4]. Although they belong to the thionin family, viscotoxins are devoid of antimicrobial activity, but they do display cytotoxic effects towards tumour cells [5–8], together with immunomodulating properties [9,10]. In addition, these proteins are weakly haemolytic [11]. These anti-tumoral properties are of particular interest since viscotoxins occur in some mistletoe-derived medicines used in anti-cancer therapy.

Viscotoxins A2, A3 and B (VA2, VA3 and VB respectively) are among the most abundant viscotoxin isoforms that occur in these mistletoe preparations [12]. Although these isoforms share a high degree of amino-acid-sequence similarity (> 90 %), they are strikingly different from each other by their *in vitro* cytotoxic potency towards Yoshida sarcoma cells: the ED_{50} (50 % efficiency diminution) recorded for VA3 (0.06 μM) is 3.5-fold (0.21 μM) and 15-fold (0.92 μM) lower than the ED_{50} measured for VA2 and VB respectively [5]. The cellular toxicity of thionins most probably results from their ability to interact with the plasma membrane [2,3,13–16]. In this respect, we have shown previously that VA3 strongly interacts with model membranes containing the acidic phospholipid phosphatidylserine (PS) [11]. According to the fact that undifferentiated tumorigenic eukaryotic cells express 7–8-fold more PS in the outer leaflet of the plasma membrane than their non-tumorigenic counterparts [17,18], we focused on the specific interaction of VA3 with this acidic phospholipid. The efficiency of VA3 to permeabilize PS vesicles was closely related to their electrostatically driven embedding in the PS head group region of the vesicles. This embedding process induced an overall stiffening of the bilayer that generates some membrane defects increasing the vesicle's susceptibility to destabilization.

To account for the *in vitro* cytotoxicity discrepancies observed for the different viscotoxins (VB, VA2 and VA3), i.e. to understand their various modes of action toward the plasma membrane, the knowledge of their main structural features is crucial. However, to date, VA3 is the only viscotoxin whose 3D structure has been solved [4]. In the present paper, we provide the NMR 3D structure determination of viscotoxins VA2 and VB. We also show that VB, VA2 and VA3 have different affinities and induce various perturbations on 1-palmitoyl-2-oleoyl-*sn*-glycero-3-phospho-L-serine (POPS) model membranes. In fact, in spite of the highly conserved overall 3D structure of the three isoforms, some significant discrete structural features, combined with distinct surface properties, account for the different affinities and perturbations observed on model membranes. If VA3 and VA2 interact in a similar way (the weaker hydrophobic character of VA2 is assumed

Abbreviations used: 3D, three-dimensional; DPH, 1,6-diphenyl-1,3,5-hexatriene; ED_{50}, 50% efficiency diminution; $LUVET_{100}$, large unilamellar vesicles of approx. 100 nm; nOe, nuclear Overhauser enhancement; POPS, 1-palmitoyl-2-oleoyl-*sn*-glycero-3-phospho-L-serine; PS, phosphatidylserine; VA2, viscotoxin A2; VA3, viscotoxin A3; VB, viscotoxin B.

[1] These authors contributed equally to this work.

[2] To whom correspondence should be addressed (e-mail andre.lopez@ipbs.fr).

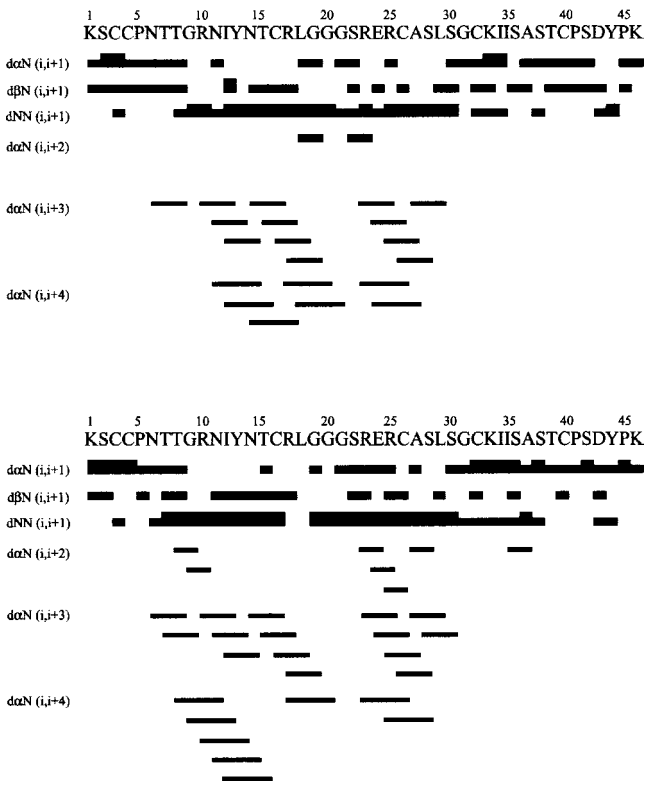

Figure 1 VA2 and VB amino-acid sequences and nOe

Amino-acid sequences and surveys of the sequential assignments of VA2 (upper panel) and VB (lower panel). The intensities of sequential nOe, extracted from NOESY with mixing times of 80 ms, are represented by bar thicknesses.

to be responsible for its apparent different affinity towards membranes), VB is much less active than the other two viscotoxins and does not insert into model membranes. A single residue (Arg^{25}) protruding outside the hydrophobic plane formed by the two amphipathic α-helices is a striking difference between VB and the other viscotoxins, disrupting the VB–membrane interaction and so seems responsible for this difference of behaviour. These different structural features that correspond to various membrane action modes could probably explain the different level of toxicity of the viscotoxins VA3, VA2 and VB.

MATERIALS AND METHODS

Chemicals

POPS was purchased from Avanti Polar Lipids (Alabaster, AL, U.S.A.). 1,6-Diphenyl-1,3,5-hexatriene (DPH) was from Molecular Probes (Eugene, OR, U.S.A.). Other chemicals were of analytical grade. VA3, VA2 and VB were isolated and purified from European mistletoe (*Viscum album*) leaves as described in [5]. VA3 stock solutions and all other aqueous solutions were gravimetrically prepared with MilliQ (Millipore) ultrapure water. POPS was stored as stock solutions in chloroformic solution (chloroform/methanol, 9:1, v/v) and was used within 24 h. Lipid purity was routinely controlled by TLC on silica gel plates with chloroform/methanol/water (65:25:4, by vol.) as the eluent. Phospholipid concentrations were estimated by phosphate assay subsequent to total digestion in the presence of perchloric acid [19].

Structure determination of VA2 and VB in solution by two-dimensional ^{1}H-NMR

For sample preparation, 8 mg of VA2 and 5 mg of VB were individually dissolved in 0.5 ml $H_2O/^2H_2O$ (9:1, v/v), pH 3 or pH 7.5, uncorrected for isotopic effect. All ^{1}H-NMR spectra were recorded on a Bruker DRX 500 spectrometer equipped with a HCN probe and self-shielded triple-axis gradients. The experiments were performed at 283 K. Two-dimensional spectra were acquired using the states-TPPI (time-proportional phase incrementation) method to achieve F1 quadrature detection [20]. Water suppression was achieved using pre-saturation during the relaxation delay (1.5 s), and during the mixing time in the case of NOESY experiments. NOESY spectra were acquired using mixing times of 80 ms [this time was selected after checking of the independence of the nuclear Overhauser enhancement (nOe) values following this parameter]. Clean-TOCSY was performed with a spin-locking field strength of 8 kHz and a spin-lock time of 80 ms.

Identification of amino-acid-residue spin systems and sequential assignment were performed using the standard strategy described by Wüthrich [21], applied with XEASY graphical software [22]. The TOCSY spectra recorded in water gave the spin-system signatures of the protein. The spin systems were then sequentially connected using the NOESY spectra.

Integration of nOe data was performed by measuring the peak volumes. On the basis of known distances in regular secondary structures ($d_{H\alpha\text{-}H\alpha} = 0.23$ nm and $d_{HN\text{-}HN} = 0.33$ nm between two strands of an antiparallel β-sheet), these volumes were translated into upper-limit distances by the CALIBA routine of DIANA [23] software. The lower limit was systematically set at 0.18 nm.

For structure calculations, distance-geometry calculations were performed with the variable target function program DIANA 2.8. A preliminary set of 1000 structures was initiated including only intra-residual and sequential upper-limit distances. From these, the best 500 were kept for a second round, including medium-range distances, and the resulting best 250 for a third round, with the whole set of upper-limit restraints, and some additional distance restraints, used to define the disulphide bridges (i.e. $d_{S\gamma,S\gamma} = 0.21$ nm, $d_{C\beta,S\gamma}$ and $d_{S\gamma,C\beta} = 0.31$ nm). Starting from the 50 best structures, a REDAC strategy [24] was finally used to include the additional distance restraints coming from hydrogen bonds determined by visual detection after the determination of the amide proton exchange rates: a 2 mM sample was freeze-dried twice and solubilized in 100 % ^2H_2O. Immediately after solubilization, a series of NOESY spectra with a mixing time of 80 ms were recorded at 300 K; the first one during a time period of 1 h, followed by spectra of 5 h each. Final energy refinement was achieved by CNS [25]. The visual analysis was performed using the TURBO software [26] and the geometric quality of the structures obtained was assessed by PROCHECK 3.3 and PROCHECK-NMR software [27].

Monolayer experiments

Isochoric measurements were performed in a circular Teflon trough with a 16 cm^2 area containing 10 ml of subphase [standard buffer: 10 mM Mops, 150 mM NaCl, 1 mM EDTA and 0.02 % (w/w) sodium azide, pH 7.4], by use of a Wilhelmy platinum plate connected to a home-made electrical torsion balance to measure the surface pressure. The atmosphere was saturated with water to prevent evaporation of the subphase during the experiment, and the temperature was maintained at 21 ± 2 °C. POPS films with a controlled initial surface pressure were obtained by successively depositing the assayed chloroformic lipid solution. After a lag time of 30 min to allow the evaporation of the solvent and

Table 1 Global root mean square deviation (RMSD) and structural statistics for the 20 best structures of VA2 and VB obtained by distance geometry and minimization

Statistic		VB		VA2	
RMSD* (Å)	Backbone atoms	0.87 ± 0.23		0.55 ± 0.17	
	All heavy atoms	1.56 ± 0.23		1.12 ± 0.18	
		(DG)†	⟨DG⟩‡	(DG)	⟨DG⟩
Energy (kcal/mol)§	Total	74.39	70.10	62.26	56.80
	Bond	3.35	4.81	3.84	3.35
	Angle	31.58	17.40	25.03	23.68
	Improper	2.70	4.95	2.30	1.99
	Van der Waals	22.28	30.91	15.80	14.06
	nOe	14.30	13.91	15.20	13.73
	Dihedral	0.18	0.45	–	–
RMSD	Bond (Å)	0.23×10^{-2}	0.15×10^{-2}	0.24×10^{-2}	0.23×10^{-2}
	Angle (°)	0.41	0.47	0.37	0.36
	Improper (°)	0.23	0.33	0.21	0.20
	Dihedral (°)	31.23	32.00	31.46	30.35
	CDihedral (°)	0.29	0.29	–	–
	nOe (Å)	0.017	0.021	0.016	0.015

* The RMSD values were calculated with respect to the mean structure. The given numbers for the backbone and all heavy atoms represent the mean pair-wise values ± S.D.
† DG represents the final 20 VA2 and 20 VB structures obtained by distance geometry and energy minimization.
‡ ⟨DG⟩ is the mean structure obtained by taking the mean of the co-ordinates of the individual DG structures that are best fitted to each other.
§ 1 kcal/mol ≈ 4.184 kJ/mol.

equilibration of the surface pressure, 10 μl of 0.1 or 1 mM viscotoxin stock solutions was introduced below the lipidic monolayer through a side hole using a syringe (10 μl; Hamilton, Bonaduz, Switzerland) and followed by 2 min of gentle stirring. The evolution of the surface pressure was recorded as a function of time, until it reached the equilibrium.

Compression isotherms were obtained as previously described in [11], by use of a laboratory-made apparatus and a Wilhelmy platinum plate to determine the surface pressure.

Fluorescence polarization

Fluorescence polarization was measured on a laboratory-made automatic T-format apparatus, as described in [11]. Large unilamellar vesicles of approx. 100 nm ($LUVET_{100}$) labelled with DPH ($\lambda_{exc} = 358$ nm, $\lambda_{em} = 428$ nm) were prepared by the extrusion method of Hope et al. [28]. The operating mode of their preparation and the characterization of their size dispersion were described in [11]. A $LUVET_{100}$ suspension was diluted in standard buffer to obtain a lipid concentration of 30 μM. The absorbance at 428 nm (A_{428}) of the lipid samples was < 0.08. Different amounts of the three viscotoxins were added to the $LUVET_{100}$ suspension and, after incubation at 21 ± 2 °C for 10 min with constant stirring, samples were put in a thermostat-controlled housing device (Peltier unit) so that the temperature of the samples could be monitored. In one set of experiments, the measurement was performed at 21 °C; in another set of experiments, the temperature was raised stepwise from 2 to 23 °C at a rate of 0.5 °C every 3 min. Fluorescence anisotropy is given by $A = (F_V + F_H)/(F_V + 2F_H)$, where F is the fluorescence intensity, and the subscripts indicate the vertical (V) or horizontal (H) orientation of the emission polarizer.

RESULTS

^{1}H-NMR 3D structures of VA2 and VB

The 3D solution structures of VA2 and VB have been solved by the ^{1}H-NMR technique. The qualitative analysis of sequential nOe intensities (Figure 1) for secondary-structure determination, together with the pattern of medium-range constraints, allowed us to predict a helix/helix conformation for both viscotoxins (from Thr^7 to Arg^{17} and from Arg^{23} to Ser^{30} for VA2; from Thr^7 to Leu^{18} and from Arg^{23} to Ser^{30} for VB). Both viscotoxins exhibit some strong sequential HN(i)-HN(i + 1), weak or no Hα(i)-HN(i + 1), and a stretch of medium-range nOe in these regions. Additionally, two extended stretches of strong Hα(i)-HN(i + 1) together with weak HN(i)-HN(i + 1) sequential nOe were detected in both toxins (from Lys^1 to Cys^4 and from Ser^{32} to Ile^{36} for VA2; from Cys^3 to Cys^4 and from Lys^{35} to Ile^{36} for VB). The 3D structures of both viscotoxins were then determined by using 787 nOe-based distance restraints (271 intra-residue, 185 sequential, 159 medium-range and 172 long-range restraints) for VA2, and 531 nOe-based distance restraints (190 intra-residue, 146 sequential, 81 medium-range and 114 long-range restraints) for VB. In addition, we used 21 (VA2) or 16 (VB) hydrogen-bond restraints and nine distance restraints derived from the three disulphide bridges. Altogether, the final experimental set corresponds to 18.21 (VA2) and 12.43 (VB) constraints per residue. The structures were calculated by using a hybrid distance-geometry-simulated annealing protocol (DIANA software) and energy refined using CNS software. The values of RMSD for VA2 and VB and a summary of the structural statistics are given in Table 1. All the solution structures have a good non-bonded contact, and covalent geometry. The best fits are shown in Figure 2. Spectra recorded at pH 3 and pH 7.5 did not present any considerable differences. The degree of ionization of the lateral chains did not change the conformation of strongly structured peptides as viscotoxins.

Structure description

Both 3D structures are very similar and exhibit the same overall fold as VA3 and other thionins (crambin or α1-purothionin) whose shape is described as a Greek capital gamma (Γ) [1]. They contain two extended α-helices (Thr^7 to Arg^{17} and Arg^{23}

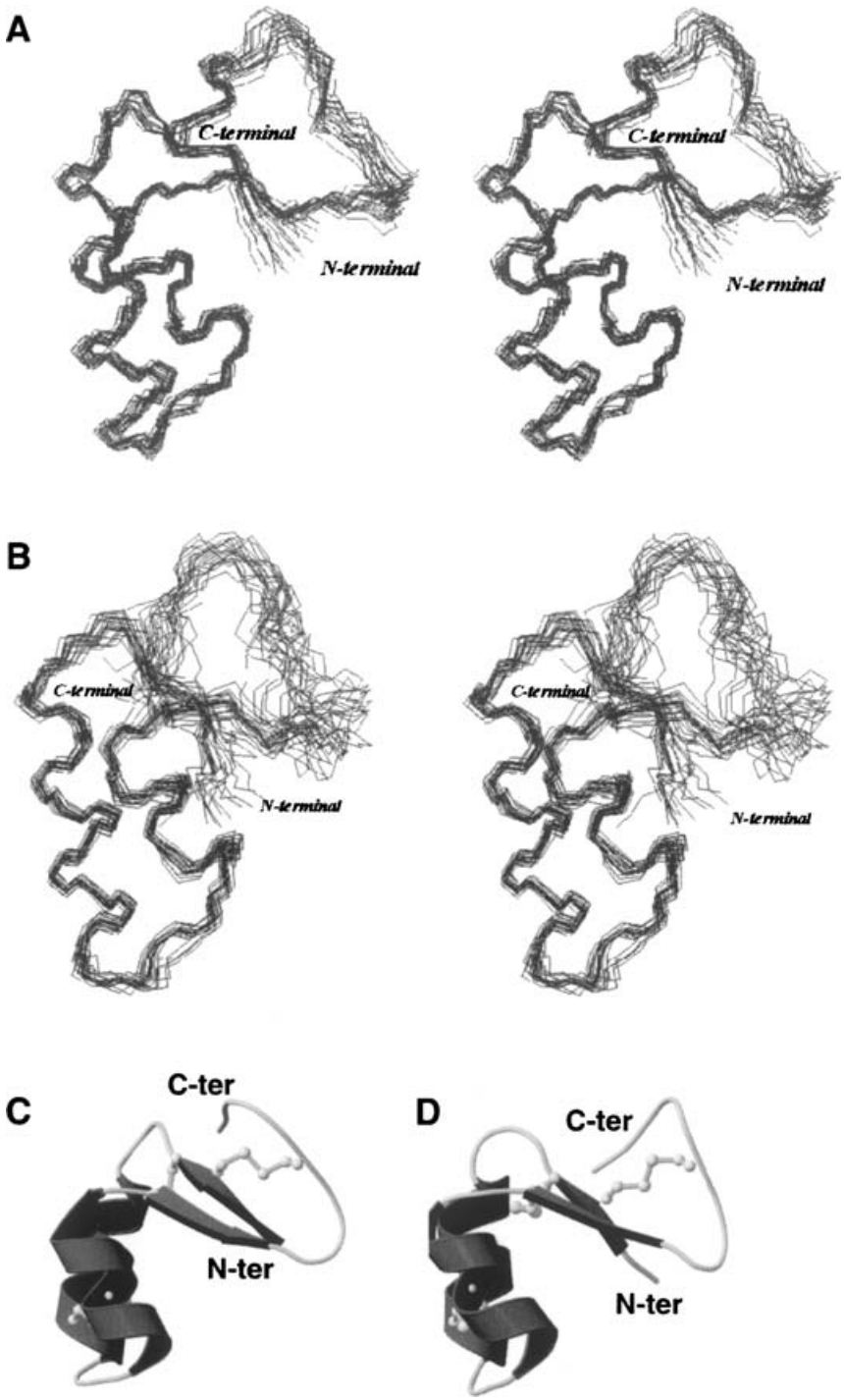

Figure 2 Stereo views of the 25 best molecular backbone structures

VA2 (**A**), VB (**B**), and MolScript representation of VB (**C**) and VA2 (**D**). Loops are shown in light grey, α-helices are shown as flat black helical ribbons and β-sheets are shown as flat black pointing in the N-terminal (N-ter) or C-terminal (C-ter) direction. Disulphide bridges are shown as ball-and-stick representations.

to Ser[30]) and two short antiparallel stretches of β-sheet (Ser[2] to Cys[3] and Lys[33] to Ile[34]) located in the two branches of the Γ respectively (Figure 2). Analysis of the 3D solution structure of VA2 and VB reveals that the angle between the axis of the α-helix and the β-sheet is similar to that observed in other thionins such as crambin [1] or α_1-purothionin [29]. The surface area occupied by hydrophobic residues (alanine, proline, isoleucine, leucine, valine and phenylalanine) amounts for 21 % (VB) and 25 % (VA2) of the total accessible surface respectively. Almost half of these hydrophobic surfaces (47 % for VB, 49 % for VA2) lie upon the plane formed by the α-helices (Table 2 and Figure 3). Hydrophobic residues of VA3, which account for 31 % of the total accessible surface, are similarly distributed (55 % upon the α-helix plane). As charged residues are mainly concentrated

Table 2 Characterization of viscotoxin residues

The data reported are the means of the data collected on the ten best structures of each viscotoxin.

	Hydrophobic residues present upon the helical stem of the two α-helices of the three viscotoxins			Number of hydrophobic and charged residues in the primary sequence of the three viscotoxins and corresponding 3D accessible areas			
	Hydrophobic residue		Accessible area of the corresponding hydrophobic residues* (Å^2)	Accessible area‡ (Å^2)		Residues§	
Viscotoxin	Upon the first helix	Upon the second helix		Hydrophobic¶	Charged‖	Hydrophobic	Charged
VA3†	Ile^{12}, Ala^{15}, Leu^{18}	Pro^{22}, Leu^{29}	499 (50 %)	915 (30 %)	746 (25 %)	13 (28 %)	8 (17 %)
VA2	Ile^{12}, Phe^{18}	Val^{25}, Leu^{29}	400 (38 %)	812 (25 %)	724 (22 %)	11 (24 %)	7 (15 %)
VB	Ile^{12}, Leu^{18}	Leu^{29}	315 (28 %)	665 (21 %)	1032 (32 %)	10 (22 %)	9 (20 %)

* Percentages were with 100 % being the accessible area of the underside of the two helices.
† The data concerning VA3 were obtained using the solution structure determined by NMR and deposited in the Protein Data Bank (id. code 1Ed0).
‡ Percentages were calculated with 100 % being the total accessible area equal to 3033, 3260 or 3215 Å^2 respectively for VA3, VA2 and VB.
§ Percentages were calculated with 100 % being the 46 residues of the primary sequences.
¶ Hydrophobic residues : phenylalanine, valine, alanine, leucine, isoleucine and proline.
‖ Charged residues : lysine, arginine, glutamic acid and aspartic acid.

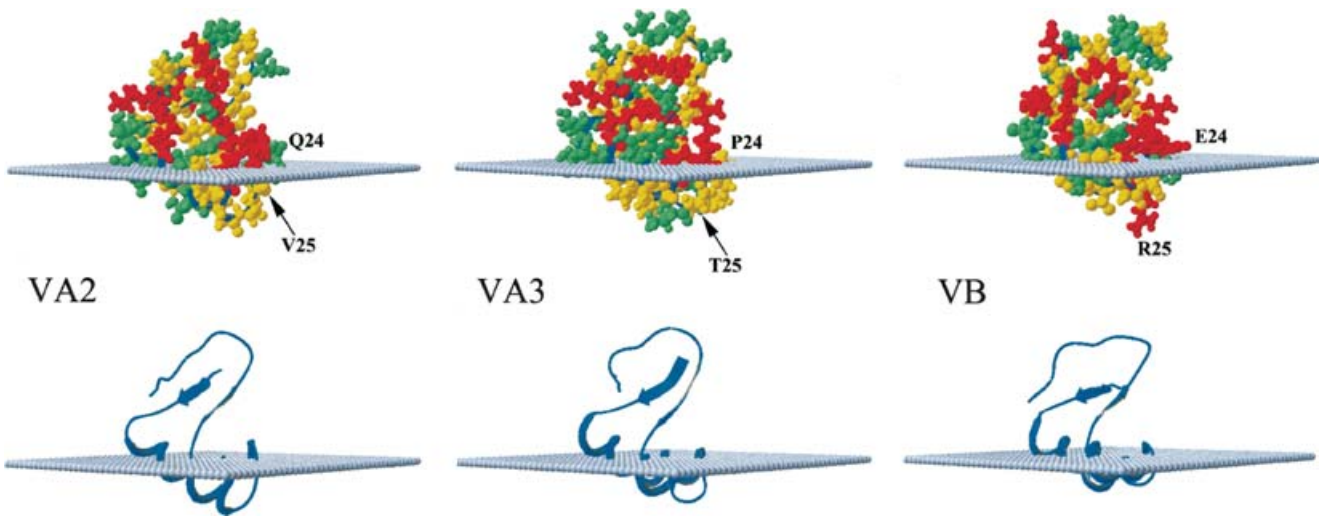

Figure 3 Amino-acid side-chain distribution in VA2 (left), VA3 (middle) and VB (right)

Residues are coloured according to their physicochemical characteristic, i.e. charged residues in blue, hydrophobic residues in yellow and polar residues in green. The plane defined by the two α-helices of the three viscotoxins is also represented. Upper panels: ball-and-stick representations of the whole viscotoxins. Residues 24 and 25 are pinpointed. Lower panel: representation of the ribbons of the three viscotoxins.

on the opposite side of the α-helix plane, this reinforces the amphipathic character of the α-helices. As previously assumed for other thionins [1,29,30], viscotoxins may interact with membranes with these amphipathic α-helices lying parallel to the plane of the phospholipid bilayer (Figure 3).

Insertion of viscotoxins in model membranes

Isochoric experiments using POPS monolayers were performed to assess the insertion of the viscotoxins into a model membrane. The addition of each viscotoxin (0.1 μM) into the subphase increased the surface pressure of weakly ordered preformed POPS films ($\pi^o \leqslant 15$ mN/m) (Figure 4). However, the insertion was less efficient in more ordered POPS monolayers of increased initial surface pressure ($\pi^o \geqslant 25$ mN/m). According to their insertion efficiency, the three viscotoxins can be classified in the following decreasing order: VA3 > VA2 > VB. It is noteworthy that viscotoxins have been similarly classified with regard to their cytotoxic effects on tumour cells [5].

The unusual shape of the $\Delta\pi = f(\pi^o)$ curve obtained for VB, which exhibits a saturation occurring at $\pi^o \leqslant 20$ mN/m, results from the weaker partition of this toxin between the bulk and the acidic lipidic phase compared with the two other viscotoxins. This cannot be related to electrostatically driven forces, as VA2 and VB bear the same net charge (+5), but it is most probably due to the different hydrophobic/hydrophilic balance of the viscotoxins, as we previously reported for VA3 [11]. The different affinity of the three viscotoxins for the air/water interface (1.0 μM) supports this hypothesis (Figure 5). It should be noted that the apparent weaker partition of 0.1 μM VA3 toward the bulk and the air/water interface is most probably due to the strong adsorption of this toxin on the cuvette walls [11], which is further proof of the strong amphiphilic character of this toxin. Likewise, the lower slope of the $\Delta\pi = f(\pi^o)$ curve obtained with 0.1 μM VA3 compared with 0.1 μM VA2 is most likely a consequence of the strong adsorption of VA3 [11].

The critical surface pressure π_c of POPS films, above which no more viscotoxin penetrates into the monolayer, can be estimated

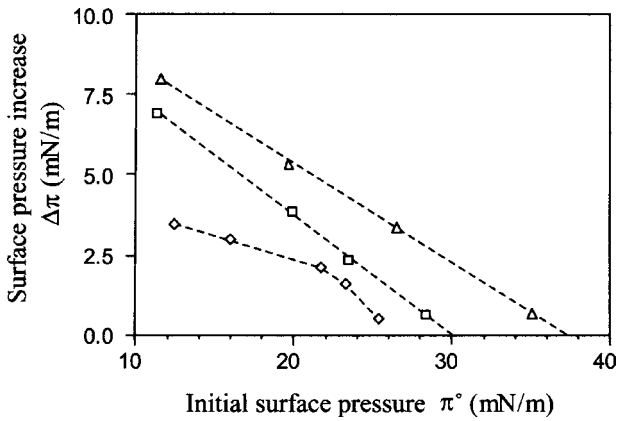

Figure 4 Increase in surface pressure of preformed POPS monolayer films

VA3 (△), VA2 (□) or VB (◇) was added (at 0.1 μM) to the subphase. Increments in surface pressure ($\Delta\pi$) are reported as a function of the initial pressure of the monolayer ($\pi°$).

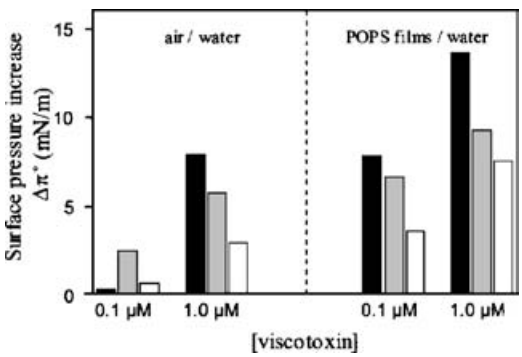

Figure 5 Increase in surface pressure upon adding 0.1 or 1 μM VA3 (black), VA2 (grey) or VB (white) to the subphase with or without a POPS film at the interface

The initial pressure of the lipidic film was 12.5 mN/m.

Table 3 Values of the critical surface pressure (π_c) for 0.1 or 1.0 μM viscotoxin in the subphase

Viscotoxin	π_c* (mN/m) at 0.1 μM viscotoxin	π_c (mN/m) at 1.0 μM viscotoxin
VA3	37.1	39.6
VA2	30.0	32.3
VB	26.1	27.0

*π_c is equal to the initial pressure of a POPS film above which the penetration of the viscotoxin is abolished. It is obtained by extrapolation of $\Delta\pi = f(\pi°)$ curves at $\Delta\pi = 0$.

from the isochoric measurements (Table 3). When compared with the equivalent surface pressure usually reported for vesicles (from 25 mN/m [31] to 32 mN/m [32]), the higher values calculated for VA3 and VA2 suggest that both toxins can penetrate into the monolayer. This is more doubtful for VB, which exhibits lower π_c values ($\leqslant$ 27 mN/m). Results obtained from compression isotherms (results not shown) are in full agreement with this assumption.

In a previous study dealing with VA3, we showed by means of isochoric measurements and release assays on LUVET$_{100}$ that the efficiency of bilayer permeabilization and monolayer penetration was directly related [11]. No permeabilization of pure POPS

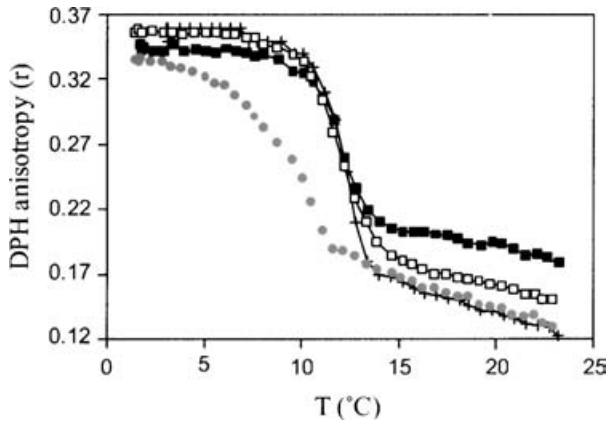

Figure 6 VA2-induced changes in the fluorescence anisotropy of a DPH probe incorporated into POPS LUVET$_{100}$ as a function of temperature

The anisotropy was measured without VA2 (●) in the subphase or with VA2 at 30 (+), 45 (□) or 52.5 μM (■). The indicated toxin concentrations are only apparent concentrations [11]. The total lipid concentration was 30 μM.

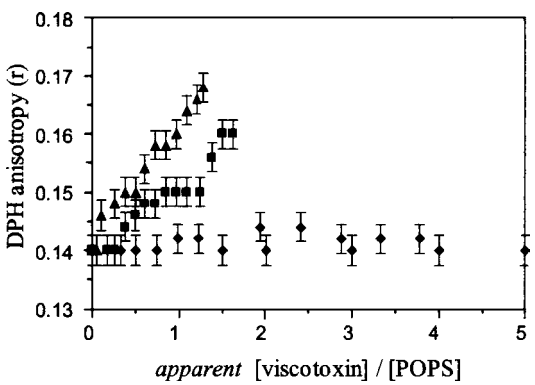

Figure 7 Changes in the fluorescence anisotropy measured at 21°C of a DPH probe incorporated into POPS LUVET$_{100}$

Various amounts of VA3 (▲), VA2 (■) or VB (◆) were added into the bulk phase. The total lipid concentration was 30 μM.

vesicles was recorded (related to a very weak penetration into POPS monolayer films), whereas incorporation of POPS in the bilayer strongly increased the efficiency of release [11]. Recording pure POPS phospholipidic vesicles release, a similar relation was obtained: although VA2 induced a significant release slightly weaker than that of the VA3, on the other hand, a very weak one was observed with VB (results not shown).

Viscotoxins modify the supramolecular organization of model membranes

As reported for VA3 [11], monitoring of the emission of a DPH probe inserted into the bilayer of POPS LUVET$_{100}$ under a polarized excitation light in the presence of increasing concentrations of VA2 showed that VA2 (i) increases the constraint of the probe in the phospholipidic gel phase, (ii) strongly increases the co-operativity of the gel to fluid transition and (iii) depending on the amount of toxin added, induces an increase of the fluorescence anisotropy of the probe when the bilayer is in a fluid state (Figure 6). However, this latter effect, which has been related to drastic perturbation of vesicles, leading to bilayer disruption [11], required a higher concentration of VA2 (Figure 7) when compared

with that induced by VA3. VB exhibited very similar effects on both the gel-phase phospholipid organization and the transition co-operativity (results not shown), but was unable to alter the fluid-phase phospholipid organization, whatever the concentration of the toxin used (Figure 7). Since the viscotoxins were found not to modify the excited-state lifetime of DPH above and below the gel-to-fluid-transition temperature (results not shown), the recorded variations of DPH anisotropy mostly reflect an overall stiffening of the bilayer induced by the toxins.

DISCUSSION

VA3 and VA2 interacted similarly on POPS supramolecular assemblies, as shown from both monolayer and fluorescence polarization experiments. The only difference observed between VA3 and VA2 concerns the larger amount of the latter toxin necessary to trigger a similar increase of the DPH anisotropy above the gel-to-fluid-transition temperature of the POPS bilayer. Obviously, the overall conformation of the viscotoxins is not responsible for this discrepancy, since both toxins do not markedly differ in this respect. More discrete structural features have to be considered. Calculation of the average accessible surface of hydrophobic residues (alanine, proline, isoleucine, leucine, valine and phenylalanine) underneath the two α-helices gives a 25% higher value for VA3 when compared with VA2 (Table 2). VA3 similarly exhibits a total hydrophobic surface 13% higher than that calculated for VA2. This discrepancy fully accounts for the higher affinity of VA3 for weakly organized POPS films, a property mainly ascribed to a chemical two-phase-partition process, as reported in [11]. In addition, VA3 exhibits a $+6$ net charge, compared with a $+5$ net charge for VA2. This electrostatic component, responsible for both the anchoring of the viscotoxins into the POPS bilayer and the stiffening of the bilayer in the vicinity of the carboxylic group of the serine heads [11], could account for the weaker penetration of VA2 in highly ordered POPS bilayers (see Table 3). However, owing to the very similar effect of VA3 and VA2 on the bilayer organization (Figure 6), the different overall hydrophobic/hydrophilic balance of the two toxins appears as the main property likely to explain their different affinity for a lipidic surrounding.

VB readily differs from the two other viscotoxins with regard to its interaction with model membranes. The very limited number of amino-acid changes occurring between VB and VA2 (Glu^{24}/Gln^{24}, Arg^{25}/Val^{25}) or VA3 (Glu^{24}/Pro^{24}, Arg^{25}/Thr^{25}, Ser^{28}/Lys^{28}) is suspected to account for this different behaviour of VB. Indeed, most of these changes correspond to exposed residues of the α-chains capable of modifying both the hydrophobic/hydrophilic balance (Glu^{24}/Gln^{24} or Arg^{25}/Thr^{25}) and the number of charged residues of the toxin (Figure 3). Accordingly, VB exhibits the lowest accessible hydrophobic surface compared with other viscotoxins (Table 2). Moreover, in spite of a net charge ($+5$) similar to VA2, this toxin possesses more charged residues (nine) than VA2 (seven) or VA3 (eight). As a result, the enhanced water-soluble character of VB reduces its affinity for the lipidic phase (Figure 4) or the air/water interface (Figure 5).

In addition, the orientation of the side-chain of Arg^{25}, which protrudes outside the plane forming the two α-helices of VB (Figure 3), acts most probably as an arm that keeps this toxin far from the lipidic interface and thus prevents its insertion into the POPS bilayer (see Figure 4). This structural feature of VB readily accounts for the absence of DPH fluorescence anisotropy increase when the phospholipidic bilayer is in a fluid state, as recorded for this toxin (Figure 7). It is noteworthy that lysine and arginine residues often stabilize the peptide/membrane interface with their long flexible aliphatic chains dipping into the hydrophobic core of the bilayer, whereas their hydrophilic heads remain in the aqueous phase or in the polar acidic head-group region [33]. However, Arg^{25} of VB cannot fulfil this role of a peptide–membrane interaction-stabilizing 'snorkel' [34,35] due to the opposite orientation of its protruding side-chain as shown on the NMR-solved 3D structure.

In summary, the different cytotoxicity displayed by VA3, VA2 and VB on tumour cells [5] obviously depends on their ability to interact with the plasma membrane and modify its supramolecular organization. Some discrete structural features of the viscotoxins and the associated surface properties readily account for their different affinity for model membranes and fully agree with their different cytotoxic potency towards tumour cells. The total accessible area occupied by hydrophobic residues (Table 2) and the accessible area of hydrophobic residues protruding from the two α-helices of viscotoxins, exhibit decreasing values along the series VA3 > VA2 > VB. In this way, these discrepancies readily account for the slightly different activity of VA3 and VA2 on model membranes. VA3 and VA2 interact with model membranes in a very similar way, but, according to the weaker hydrophobic character of VA2 that penalizes its two-phase bulk/membrane partition, a higher concentration of this toxin is necessary to induce the same effects on POPS bilayers. Although both toxins also differ by their net charges, $+6$ for VA3 compared with $+5$ for VA2, the electrostatic component seems to be less relevant in this respect, since it mainly stabilizes the interaction rather than being involved in the partition process. VB interacts in a very different way on model membranes that explains its lowest toxicity to tumour cells. Even though the lower hydrophobic character displayed by this viscotoxin (Table 2) accounts for its reduced affinity for the lipidic phase, the main structural feature responsible for the apparent lack of insertion of VB into the POPS model membrane presumably results from a single amino acid change. The occurrence of Arg^{25} protruding from the hydrophobic plane forming the two α-helices should prevent the insertion of VB into the membrane, and would explain the lowest cytotoxic activity reported for this toxin.

This work was supported by the Centre National de la Recherche Scientifique (CNRS) and the Association pour la Recherche sur le Cancer (ARC).

REFERENCES

1 Florack, D. E. and Stiekema, W. J. (1994) Thionins: properties, possible biological roles and mechanisms of action. Plant Mol. Biol. **26**, 25–37
2 Hughes, P., Dennis, E., Whitecross, M., Llewellyn, D. and Gage, P. (2000) The cytotoxic plant protein, β-purothionin, forms ion channels in lipid membranes. J. Biol. Chem. **275**, 823–827
3 Wilson, H. A., Huang, W., Waldrip, J. B., Judd, A. M., Vernon, L. P. and Bell, J. D. (1997) Mechanisms by which thionin induces susceptibility of S49 cell membranes to extracellular phospholipase A2. Biochim. Biophys. Acta **1349**, 142–156
4 Romagnoli, S., Ugolini, R., Fogolari, F., Schaller, G., Urech, K., Giannattasio, M., Ragona, L. and Molinari, H. (2000) NMR structural determination of viscotoxin A3 from *Viscum album* L. Biochem. J. **350**, 569–577
5 Schaller, G., Urech, K. and Giannattasio, M. (1996) Cytotoxicity of different viscotoxins and extracts from European subspecies of *Viscum album*. Phytother. Res. **10**, 473–477
6 Urech, K., Schaller, G., Ziska, P. and Giannattasio, M. (1995) Comparative study on the cytotoxic effect of viscotoxin and mistletoe lectin on tumor cells in culture. Phytother. Res. **9**, 49–55
7 Jung, M. L., Baudino, S., Ribereau-Gayon, G. and Beck, J. P. (1990) Characterization of cytotoxic proteins from mistletoe (*Viscum album* L.). Cancer Lett. **51**, 103–108
8 Konopa, J., Woynarowski, J. M. and Lewandowska-Gumieniak, M. (1980) Isolation of viscotoxins. Cytotoxic basic polypeptides from *Viscum album* L. Hoppe Seyler's Z. Physiol. Chem. **361**, 1525–1533
9 Bussing, A., Vervecken, W., Wagner, M., Wagner, B., Pfuller, U. and Schietzel, M. (1999) Accidental cell death and generation of reactive oxygen intermediates in human lymphocytes induced by thionins from *Viscum album* L. Cytometry **37**, 133–139

10 Bussing, A., Stein, G. M., Wagner, M., Wagner, B., Schaller, G., Pfuller, U. and Schietzel, M. (1999) Expression of mitochondrial Apo2.7 molecules and caspase-3 activation in human lymphocytes treated with the ribosome-inhibiting mistletoe lectins and the cell membrane permeabilizing viscotoxins. Eur. J. Biochem. **262**, 79–87
11 Coulon, A., Berkane, E., Sautereau, A. M., Urech, K., Rouge, P. and Lopez, A. (2002) Modes of membrane interaction of a natural cysteine-rich peptide: viscotoxin A3. Biochim. Biophys. Acta **1559**, 145–159
12 Schaller, G., Urech, K., Grazi, G. and Giannattasio, M. (1998) Viscotoxin composition of the three European subspecies of *Viscum album*. Planta Medica **64**, 677–678
13 Evans, J., Wang, Y. D., Shaw, K. P. and Vernon, L. P. (1989) Cellular responses to *Pyrularia* thionin are mediated by Ca^{2+} influx and phospholipase A2 activation and are inhibited by thionin tyrosine iodination. Proc. Natl. Acad. Sci. U.S.A. **86**, 5849–5853
14 Osorio e Castro, V. R. and Vernon, L. P. (1989) Hemolytic activity of thionin from *Pyrularia pubera* nuts and snake venom toxins of *Naja naja* species: *Pyrularia* thionin and snake venom cardiotoxin compete for the same membrane site action of a thionin isolated from nuts of *Pyrularia pubera* on human erythrocytes. Toxicon **27**, 511–517
15 Thevissen, K., Ghazi, A., De Samblanx, G. W., Brownlee, C., Osborn, R. W. and Broekaert, W. F. (1996) Fungal membrane responses induced by plant defensins and thionins. J. Biol. Chem. **271**, 15018–15025
16 Caaveiro, J. M., Molina, A., Gonzalez-Manas, J. M., Rodriguez-Palenzuela, P., Garcia-Olmedo, F. and Goni, F. M. (1997) Differential effects of five types of antipathogenic plant peptides on model membranes. FEBS Lett. **410**, 338–342
17 Connor, J., Bucana, C., Fidler, I. J. and Schroit, A. J. (1989) Differentiation-dependent expression of phosphatidylserine in mammalian plasma membranes: quantitative assessment of outer-leaflet lipid by prothrombinase complex formation. Proc. Natl. Acad. Sci. U.S.A. **86**, 3184–3188
18 Utsugi, T., Schroit, A. J., Connor, J., Bucana, C. D. and Fidler, I. J. (1991) Elevated expression of phosphatidylserine in the outer membrane leaflet of human tumor cells and recognition by activated human blood monocytes. Cancer Res. **51**, 3062–3066
19 McClare, C. W. (1971) An accurate and convenient organic phosphorus assay. Anal. Biochem. **39**, 527–530
20 Marion, D. and Wuthrich, K. (1983) Application of phase sensitive two-dimensional correlated spectroscopy (COSY) for measurements of ^1H–^1H spin–spin coupling constants in proteins. Biochem. Biophys. Res. Commun. **113**, 967–974
21 Wüthrich, K. (1986) NMR of proteins and nucleic acids, John Wiley & Sons, New York
22 Bartels, C., Xia, T. H., Billeter, M., Güntert, P. and Wüthrich, K. (1995) The program XEASY for computer-supported NMR spectral analysis of biological macromolecules. J. Biomol. NMR **6**, 1–10
23 Guntert, P. and Wüthrich, K. (1991) Improved efficiency of protein structure calculations from NMR data using the program DIANA with redundant dihedral angle constraints. J. Biomol. NMR **1**, 447–456
24 Guntert, P., Braun, W. and Wüthrich, K. (1991) Efficient computation of three-dimensional protein structures in solution from nuclear magnetic resonance data using the program DIANA and the supporting programs CALIBA, HABAS and GLOMSA. J. Mol. Biol. **217**, 517–530
25 Brunger, A. T., Adams, P. D., Clore, G. M., DeLano, W. L., Gros, P., Grosse-Kunstleve, R. W., Jiang, J. S., Kuszewski, J., Nilges, M., Pannu, N. S. et al. (1998) Crystallography and NMR system: a new software suite for macromolecular structure determination. Acta Crystallogr. Sect. D. Biol. Crystallogr. **54**, 905–921
26 Roussel, A. and Cambillau, C. (1989) In Silicon Graphics Geometry Partner Directory, pp. 77–79, Silicon Graphics, Mountain View, CA
27 Laskowski, R. A., Rullmann, J. A., MacArthur, M. W., Kaptein, R. and Thornton, J. M. (1996) Aqua and Procheck-NMR: programs for checking the quality of protein structures solved by NMR. J. Biol. Mol. NMR **8**, 477–486
28 Hope, M. J., Bally, M. B., Webb, G. and Cullis, P. R. (1985) Production of large unilamellar vesicles by a rapid extrusion procedure. Characterization of size distribution, trapped volume and ability to maintain a membrane potential. Biochim. Biophys. Acta **812**, 55–65
29 Kelly, I., Pézolet, M. and Marion, D. (1998) Study of the secondary structure of purothionin-β and its interactions with phospholipids by 2D-infrared spectroscopy and infrared linear dichroism. Biophys. J. **74**, A309
30 Teeter, M. M., Ma, X. Q., Rao, U. and Whitlow, M. (1990) Crystal structure of a protein-toxin α 1-purothionin at 2.5 Å and a comparison with predicted models. Proteins **8**, 118–132
31 Schindler, H. (1979) Exchange and interactions between lipid layers at the surface of a liposome solution. Biochim. Biophys. Acta **555**, 316–336
32 Seelig, A. (1987) Local anesthetics and pressure: a comparison of dibucaine binding to lipid monolayers and bilayers. Biochim. Biophys. Acta **899**, 196–204
33 Killian, J. A. and von Heijne, G. (2000) How proteins adapt to a membrane–water interface. Trends Biochem. Sci. **25**, 429–434
34 Segrest, J. P., De Loof, H., Dohlman, J. G., Brouillette, C. G. and Anantharamaiah, G. M. (1990) Amphipathic helix motif: classes and properties. Proteins **8**, 103–117
35 de Planque, M. R., Kruijtzer, J. A., Liskamp, R. M., Marsh, D., Greathouse, D. V., Koeppe, R. E., de Kruijff, B. and Killian, J. A. (1999) Different membrane anchoring positions of tryptophan and lysine in synthetic transmembrane α-helical peptides. J. Biol. Chem. **274**, 20839–20846

Received 31 March 2003/29 April 2003; accepted 6 May 2003
Published as BJ Immediate Publication 6 May 2003, DOI 10.1042/BJ20030488